molecular pharmaceutics

Article

Cite This: Mol. Pharmaceutics 2018, 15, 4710−4721

pubs.acs.org/molecularpharmaceutics

Submicron Aggregation of Chemically Denatured Monoclonal Antibody

Jacob B. Rowe,[†,§] Rhiannon P. Flynn,[†] Harrison R. Wooten,[†] Hailey A. Noufer,[†] Rachel A. Cancel,[†] Jifeng Zhang,[‡,∥] J. Anand Subramony,[‡] Sergei Pechenov,[*,‡] and Ying Wang[*,†]

[†]Department of Chemistry and Biochemistry, University of North Carolina Wilmington, Wilmington, North Carolina 28403, United States

[‡]MedImmune, One MedImmune Way, Gaithersburg, Maryland 20878, United States

Supporting Information

ABSTRACT: Isothermal chemical denaturation (ICD) has been widely used to evaluate the conformational stability of therapeutic proteins such as monoclonal antibodies. However, the chemical unfolding pathway and the subsequent aggregation of antibodies are not yet well-understood. In the present work, we conducted a systematic study on an ICD-induced aggregation of a pharmaceutical monoclonal antibody. Using dynamic light scattering, we monitored formation and growth of submicron aggregates in various buffers. Our experiments revealed a nucleation-controlled submicron aggregation of the antibody in the presence of chemical denaturant. After the unfolded protein reached a steady state, we reduced the denaturant concentration by dilution or dialysis to trigger further aggregation after ICD. In this way, we studied the pH effect on aggregation of the stressed protein after removal of denaturant. The ICD-dilution experiment provides a practical means for studying the propensity of unfolded proteins to form aggregates under various formulation conditions. This unique method allows us to control the degree of protein unfolding and the initiation of post-ICD aggregation.

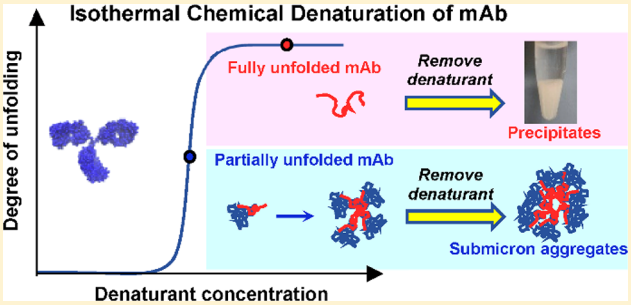

KEYWORDS: *isothermal chemical denaturation (ICD), differential scanning calorimetry (DSC), dynamic light scattering (DLS), protein unfolding, protein aggregation, submicron particles*

1. INTRODUCTION

Assessment of protein conformational stability is of great importance in the development of biologics such as monoclonal antibodies (mAbs). During production, purification, formulation, and administration, proteins are exposed to a broad range of solution environments, e.g., various concentrations, temperatures, pHs, ionic strengths, salts, excipients, etc. Under certain solution conditions, the protein may be prone to unfolding and aggregation, which not only compromises the therapeutic activity of biologics but also increases the risk of immunogenicity.[1−3] Two common approaches to evaluating protein conformational stability include thermal and chemical denaturation. A classical method to study thermal unfolding of proteins is differential scanning calorimetry (DSC). The melting temperature measured in DSC experiments can serve as a surrogate of protein conformational stability. In addition, if protein unfolding is reversible, characteristic thermodynamic quantities can be obtained from DSC experiments, providing rich information about unfolding.[4,5] However, the thermal unfolding studies are often complicated by irreversible protein aggregation.[6−8] In contrast, unfolding induced by chemical denaturants, such as urea and guanidine hydrochloride (GuHCl), usually does not cause protein precipitation. During chemical denaturation, the folded and unfolded states are considered to be in a thermodynamic equilibrium.[9−11] Isothermal chemical denaturation (ICD) monitored by fluorescence, UV, or circular dichroism, is widely used to study protein conformational stability. The standard Gibbs free energy change associated with protein unfolding without denaturant can be extrapolated from ICD measurements.[12−15] Nevertheless, a recent study shows that the results of ICD experiments on large proteins like IgG antibodies depend on the incubation time, refolding cycles, type of denaturant, and the detection methods.[16] These observations indicate that chemical denaturation of large proteins may be pathway-dependent and irreversible, even when there is no precipitation. Such irreversible unfolding of large proteins can be expected, considering their complicated free energy landscape and the numerous possible intermediate states.[17,18] To appreciate both the limitations and usefulness of

Received: July 3, 2018
Revised: August 14, 2018
Accepted: August 24, 2018
Published: August 24, 2018

DOI: 10.1021/acs.molpharmaceut.8b00690
Mol. Pharmaceutics 2018, 15, 4710−4721

ICD analysis for antibodies, further understanding of the chemical denaturation pathway is needed.

Denatured proteins in a biologics formulation may form aggregates over time during storage. However, protein conformational stability studies do not always predict the long-term stability of protein solutions. For instance, a recent study showed that the stability of various mAb formulations during storage is not directly correlated to their thermal stability measured by DSC.[8] For evaluating the long-term stability of protein formulations, it is necessary to study the aggregation pathways of the unfolded proteins. The typical kinetic mechanisms of protein aggregation include continuous aggregation and nucleation-controlled aggregation.[19,20] The two mechanisms can be differentiated by studying the early stages of aggregation using light scattering, fluorescence, and resonance mass measurements.[21,22] Unlike continuous aggregation, nucleation-controlled kinetics is characterized by a lag time of aggregation.[19,20,23] Nucleation-controlled aggregation is often observed for small proteins and peptides that undergo fibril formation, e.g., amyloid β-protein, α-synuclein, and the light chain of IgG antibodies.[24−28] For aggregation of full mAbs caused by thermal and pH stresses, both kinetic mechanisms have been proposed.[29−31] Chemical denaturation provides a unique way to study non-native protein aggregation pathways in a controlled manner. The degree of protein unfolding can be adjusted by changing denaturant concentration according to the experimental ICD curves. After protein unfolding, aggregation of the denatured protein can be initiated by lowering the denaturant concentration, either through dilution or dialysis. Using this approach, we investigated aggregation of a chemically denatured mAb in the present work.

Aggregation of denatured proteins can be affected by various factors. The effects of pH and ionic strength on the aggregation of thermally denatured IgG antibodies has previously been studied.[24,32−37] In general, IgG antibodies, particularly the C_H2 domain of the crystallizable (Fc) fragment, have lower conformational stability at low pH. On the other hand, low pH can mitigate aggregation by increasing the protein's net charge, since most IgG antibodies have a neutral or basic isoelectric point.[38−40] When protein unfolding is extensive, the electrostatic repulsion between ionized functional groups may not be enough to prevent protein aggregation. Through chemical denaturation, the degree of unfolding can be controlled by adjusting the concentration of chemical denaturant. Here, we used this approach to investigate the aggregation behavior of partially and fully unfolded IgG mAb and how this behavior changes at different pHs.

The present work provides insights into the aggregation of a therapeutic mAb during chemical denaturation. We found that chemical denaturation of this IgG is an irreversible process, similar to that of thermal denaturation. Therefore, the simple ICD equilibrium models are not suitable for rigorous thermodynamic analysis of protein unfolding in antibody formulations. In addition, we observed a nucleation-controlled submicron aggregation of this antibody. At last, chemical denaturation of IgGs and subsequent removal of denaturant provides a practical way to evaluate the effects of formulation condition, such as pH, on aggregation of denatured biologics during storage.

2. MATERIALS AND METHODS

2.1. Proteins, Chemicals, and Solution Preparation. A human IgG1 subclass monoclonal antibody denoted as mAbX was used in this study. mAbX was produced and purified at MedImmune Inc. The purity was confirmed to be >98% by size-exclusion chromatography (Superdex 200 10/300 GL, GE Healthcare, Little Chalfont, United Kingdom) and an HPLC system (Gold 126, Beckman Coulter, Brea, CA). The molecular weight of mAbX was determined to be 148 236 Da by electrospray ionization time-of-flight (ESI-TOF) mass spectrometry (microTOF II, Bruker, Billeria, MA). The isoelectric point of mAbX is 8.1 (MedImmune internal data). Two other proteins, lysozyme and bovine serum albumin (BSA), were used to compare unfolding and aggregation of proteins with different sizes. The ultrapure-grade hen egg-white lysozyme was purchased from Amresco (VWR, Dallas, TX). The fatty-acid-free 98% BSA (Cohn fraction V) was purchased from Alfa Aesar (Haverhill, MA). The theoretical molecular weights are 14 313.14 Da for lysozyme and 66 432.96 Da for BSA (calculated using ProParam, www.expasy.org). The experimental isoelectric points were previously reported to be pI 11 for lysozyme[41] and pI 5.3 for the fatty-acid-free BSA.[42] The chemicals used to prepare buffers include sodium acetate trihydrate 99.0−100.5% (Alfa Aesar, Havehill, MA), glacial acetic acid (Thermo Fisher Scientific, Fairlawn, NJ), histidine >98% (ACROS Organics, Morris Plains, NJ), 6 M hydrochloric acid, sodium phosphate monobasic monohydrate 98−102%, and sodium phosphate dibasic anhydrous 98−105% (Thermo Fisher Scientific, Fairlawn, NJ). The chemical denaturant GuHCl was purchased from Thermo Fisher Scientific (Fairlawn, NJ).

Three buffers used in this work are 20 mM sodium acetate at pH 5.00 ± 0.02, 20 mM histidine hydrochloride at pH 6.02 ± 0.02, and 20 mM sodium phosphate at pH 7.01 ± 0.02. To prepare the protein stock solutions, the original mAbX solutions were exhaustively dialyzed into the desired buffer using a diafiltration stirred cell (Amicon, EMD Millipore, Billerica, MA) with ultrafiltration membrane discs (Ultracel 10 kDa, EMD Millipore, Billerica, MA). The protein solutions were further concentrated using a centrifugal filter (50 kDa Amicon ultra-4, Merck Millipore, Cork, Ireland). The lysozyme and BSA stock solutions were prepared by dissolving the crystalline powders in the buffer. The protein stock solutions were used to prepare the samples for analysis. The final protein concentrations of samples were measured by UV absorbance at 280 nm using extinction coefficients 1.35 $L{\cdot}g^{-1}{\cdot}cm^{-1}$ for mAbX (MedImmune internal data), 2.618 $L{\cdot}g^{-1}{\cdot}cm^{-1}$ for lysozyme (calculated using ProParam), and 0.614 $L{\cdot}g^{-1}{\cdot}cm^{-1}$ for BSA (calculated using ProParam). GuHCl stock solutions were prepared by dissolving the salt in each buffer. Since GuHCl is hygroscopic, the accurate denaturant concentration was determined using a white-light refractometer (ABBL-3L, Bausch & Lomb, USA) and a calibration curve $C_d = 57.147\Delta n + 38.68\Delta n^2 - 91.6\Delta n^3$ where C_d is the molarity of GuHCl, and Δn is the difference between the refractive index of GuHCl solution and that of buffer.[43]

2.2. Fluorescence Measurements of ICD Curves. The ICD curves of the proteins were measured using a fluorescence microplate reader (FlexStation 3, Molecular Devices, San Jose, CA). For each protein−buffer combination, a solution A and a solution B were prepared. Solution A containing 0.3 mg/mL protein (0.6 mg/mL for BSA) was prepared by diluting 40 μL

DOI: 10.1021/acs.molpharmaceut.8b00690
Mol. Pharmaceutics 2018, 15, 4710−4721

of 30 mg/mL protein stock solution (60 mg/mL for BSA) with 3.96 mL of buffer. Solution B containing 0.3 mg/mL protein (0.6 mg/mL for BSA) and 8 M GuHCl were prepared by diluting 40 μL of 30 mg/mL protein stock solution (60 mg/mL for BSA) with 3.96 mL of 8 M GuHCl stock solution. The accurate GuHCl concentration of solution B was measured by the precalibrated refractometer. For the ICD experiment, 24 samples of each protein−buffer combination with different GuHCl concentrations ranging from 0 to 8 M and the same protein concentration were prepared by pipetting and mixing solutions A and B in 96-well microplates (UV-Star, Black, Greiner Bio-One, Monroe, NC) using an eight-channel electronic pipettor (VWR, Dallas, TX). The fluorescence emission spectra of the samples at excitation wavelength 280 nm were collected from 300 to 450 nm with a 10 nm interval. To reduce well-to-well variation, the ratio of fluorescence intensities at 350 and 310 nm was plotted versus the GuHCl concentration to obtain the ICD curves. The ICD curves were measured at 25 and 37 °C. Fluorescence spectra were measured after 0, 0.5, 6, 10, 16, and 48 h of incubation. The spectra at 48 h were used to generate the steady-state ICD curves.

2.3. Dynamic Light Scattering (DLS) Measurements of Chemically Induced Protein Unfolding and Aggregation. The size of protein particles was measured by a custom-made DLS apparatus using a coherent He−Ne laser (35 mW, 632.8 nm; Coherent Inc., Santa Clara, CA) and a correlator (PD2000 DLS PLUS, Precision Detectors, Bellingham, MA). All DLS samples were filtered using syringe filter (13 mm, 0.45 μm cellulose acetate, VWR, Dallas, TX) to remove dust and other pre-existing particles. The protein concentrations in all samples were 4 mg/mL. The samples of partially and fully unfolded proteins contained GuHCl at two concentrations determined by the ICD curves, respectively, the middle point of the transition stage and a point on the plateau of unfolding. The GuHCl concentrations in the samples were verified using the precalibrated refractometer.

The refolded protein samples were prepared in two ways as described below. In the first method, 40 mg/mL partially and fully unfolded protein solutions were incubated at 4 °C for 48 h to reach steady states, and refolding was initiated by diluting 10× with the corresponding buffer. The second method was to remove GuHCl by exhaustive dialysis against the buffer using semipermeable membrane tubing (Spectra/Por MWCO 6−8000, 10 mm, Spectrum Laboratories Inc., Rancho Dominguez, CA). Partially and fully unfolded protein solutions (1 mL volume, 4 mg/mL) were dialyzed against 1 L of buffer three times in 3 consecutive days at 4 °C in a cold room. In the DLS measurements, the light scattering intensity of the native, unfolded, and refolded protein samples were monitored at 25 °C and a scattering angle of 90°. Diffusion coefficients, D, were determined from the measured correlation function by the Precision Deconvolve 5.5 software (Precision Detectors) using a regularization algorithm. The apparent hydrodynamic radii, R_h, were calculated from D using the Stokes−Einstein equation, $R_h = kT/6\pi\eta D$, where k is the Boltzmann's constant, T is the absolute temperature, and η is the viscosity of solvent. η of the buffers with GuHCl were measured at 25 °C using a glass capillary viscometer (A223, CANNON, State College, PA).

2.4. Circular Dichroism (CD) Measurements of mAbX Structure. The secondary structures of native and refolded (dialyzed) mAbX were investigated by far-UV CD experiments. The concentrations of native protein and refolded protein samples measured by UV absorbance were 0.6 and 0.4 mg/mL, respectively. The protein solutions in 20 mM acetate and 20 mM phosphate buffers were measured. (Histidine buffer at 20 mM was not measured because of the strong absorbance in the far-UV wavelength range.) Each sample (300 μL) was placed in a 1 mm quartz cuvette (NE-1-Q-1, New Era, Vineland, NJ), and the CD spectra from 300 to 190 nm with 1 nm intervals were collected at 25 °C by a CD spectrometer (Chirascan, Applied Photophysics, Beverly, MA). The CD spectra of the buffer were subtracted from those of the sample. The mean residue ellipticity, θ, was calculated from the experimental ellipticity, θ_{obs}, using $\theta = \theta_{obs}M/cln$ where M = 148 236 Da is the molecular weight of mAbX, c is the protein mass concentration, n = 1346 is the number of amino acid residues in mAbX, and l = 0.1 cm is the path length of the cuvette.

2.5. DSC and DLS Measurements for Thermal Unfolding of mAbX. The thermal stability of mAbX was analyzed using a differential scanning calorimeter (nano DSC, TA Instruments, Lindon, UT). Protein solutions (4 mg/mL) and the reference buffers were degassed. The sample temperature was increased from 40 to 90 °C at a heat rate, p_{heat} = 0.2 °C/min, and then cooled down to 40 °C at 2 °C/min. Repeated heating showed no transition peak, suggesting protein precipitation. The excess molar heat capacity, C_P, was calculated from the measured heat flow, P_{ex}, using $C_P = P_{ex}M/p_{heat}cV$, where V = 300 μL is the sample volume of the calorimeter.

The sizes of thermally denatured mAbX in various buffers were monitored by DLS experiments. On the basis of the results of DSC experiments, 4 mg/mL mAbX samples in the three buffers were incubated in a water bath with a temperature gradient from 40 to 65 °C at 0.2 °C/min. The samples were immediately taken out of the water bath after the incubation and cooled with running tap water. This preparation procedure produced partially denatured mAbX samples. The samples were measured by DLS experiments at 25 °C.

RESULTS AND DISCUSSION

3.1. Chemical Denaturation and Conformational Stability of mAbX. Our goal of this work is to examine the reversibility and aggregation of chemically denatured mAb. To control the degree of unfolding, we determined the ICD curve of mAbX in a formulation buffer, 20 mM histidine hydrochloride at pH 6.0 (Figure 1A). The ICD curves of BSA and lysozyme in the same buffer were also determined for intuitive comparison of protein conformational stability. BSA and lysozyme are chosen here, because they are widely used as model systems for studying protein unfolding, and they also represent different-sized proteins for comparing their aggregation behavior, as shown later. Because the spectra of intrinsic protein fluorescence excited at 280 nm depends on the environment of the tryptophan residues, the change of fluorescence signals indicates a protein conformational change. Figure 1A shows that mAbX and BSA unfold at GuHCl concentrations lower than that of lysozyme. This result suggests that the conformational stability of mAbX is lower than that of lysozyme but is comparable to that of BSA, a stable serum protein. Note that the flipped shape of the ICD curve of BSA is caused by a less common blue shift of fluorescence

DOI: 10.1021/acs.molpharmaceut.8b00690
Mol. Pharmaceutics 2018, 15, 4710−4721

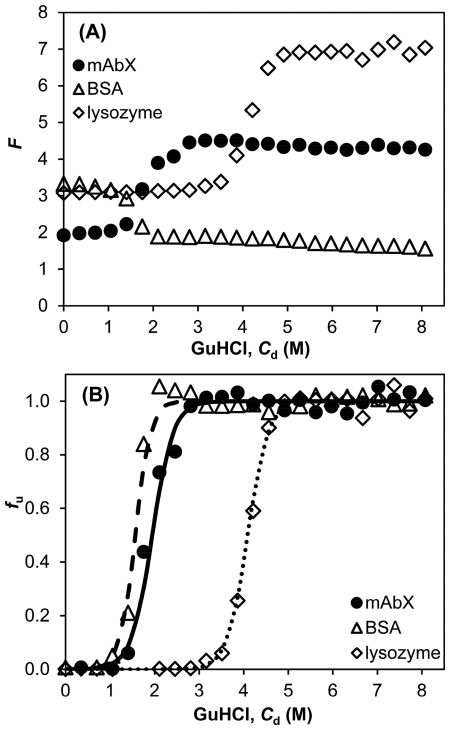

Figure 1. ICD curves of mAbX, lysozyme, and BSA in 20 mM His·HisHCl buffer at pH 6.0 and 25 °C after the proteins reached the steady state. (A) The ratio of fluorescence intensities at 350 and 310 nm as a function of denaturant concentration; (B) the fraction of unfolded proteins calculated from the data in (A). The solid, dashed, and dotted curves are the fits of experimental data using a two-state unfolding model.

light, likely a result of the solvent-accessible tryptophan residue in the ligand-binding site of BSA (Figure S1).[44,45]

We also conducted ICD experiments on the proteins in two other buffers, a 20 mM pH 5.0 acetate and a 20 mM pH 7.0 phosphate (Figure S2). We found that the pH's effect on chemical unfolding of all three proteins is insignificant. The ICD curves of each protein in different buffers overlap within the experimental uncertainties. Similarly, the effect of moderate temperature change on chemical denaturation of these proteins was examined by ICD experiments at 25 and 37 °C (Figure S3). The ICD curves of the proteins at the two temperatures are essentially the same, except for a slightly sharper transition of lysozyme unfolding at 37 °C (Figure S4). These results suggest that the conformational stability of mAbX, and maybe other protein therapeutics determined by ICD experiments is not strongly affected by pH and temperature within the most relevant formulation design space.

In ICD studies, the experimental data are often analyzed using a simple two-state model, which assumes an equilibrium is established between the native and unfolded states at a given denaturant concentration. Using this model, an unfolding Gibbs free energy can be extracted from ICD curves to quantify the conformational stability of the protein. For example, the initial and final sections of the ICD curves in Figure 1A can be fitted with two linear baselines for the native and unfolded states, respectively, $y_n = a_n + b_nC_d$ and $y_u = a_u + b_uC_d$ where C_d is the GuHCl concentration, y_n and y_u are the fluorescence signals of pure native and unfolded proteins, respectively, and a and b are the fitting parameters. Then, the observed fluorescence signal, F, in Figure 1A can be converted into the fraction of unfolded proteins, f_u, shown in Figure 1B using $f_u = (F - y_n)/(y_u - F)$. At a given GuHCl concentration, the unfolding equilibrium is described by the standard Gibbs free energy $\Delta G^o = -RT\ln\left(\frac{f_u}{1-f_u}\right)$. Previous work has shown that ΔG^ϕ is approximately a linear function of denaturant concentration, i.e., $\Delta G^\phi = \Delta G_0^\phi - mC_d$.[12−15] Here, ΔG_0^ϕ is the standard Gibbs free energy for protein unfolding without denaturant, and m is a measure of the denaturant's effect on protein unfolding.[46] Therefore, by fitting the ICD curves in Figure 1B using $\frac{f_u}{1-f_u} = e^{-(\Delta G_0^o - mC_d)/RT}$, the values of m and ΔG_0^ϕ were obtained for mAbX, BSA, and lysozyme, as shown in Table 1. The ΔG_0^ϕ of BSA and lysozyme in Table 1 is

Table 1. Results of Fitting the ICD Curves in Figure 1B Using a Simple Two-State Model

	mAbX	BSA	lysozyme
m (kJ·L/mol^2)	11 ± 1	15 ± 2	10.9 ± 0.4
ΔG_0^ϕ (kJ/mol)	21 ± 3	23 ± 3	45 ± 2
fraction of unfolded protein, f_u, without GuHCl	2.1×10^{-4}	9.3×10^{-5}	1.3×10^{-8}

consistent with the previously reported values of 20 kJ/mol for BSA at pH 6[16] and 34 kJ/mol for lysozyme at pH 9.[47] The large positive ΔG_0^ϕ of lysozyme indicates high conformational stability. ΔG_0^ϕ of mAbX and BSA are the same within experimental uncertainty. From the values of ΔG_0^ϕ, one could also estimate the apparent fraction of unfolded protein, f_u, in the solutions without denaturant. Table 1 shows that degree of unfolding of these three proteins are extremely low in the absence of chemical denaturant. Therefore, conformational stability of mAbX should not be a major concern in the formulation at ordinary ambient temperatures. That said, colloidal stability and self-association of the protein could play a more important role for formulation development.

3.2. Submicron Aggregation of mAbX in the Presence of Denaturant. ICD experiments can provide valuable information about the conformational stability of proteins. However, the a priori of the ICD thermodynamic analysis is that an equilibrium is reached between the native state and a well-defined unfolded state (or more than one unfolded state when multiple-stage ICD curves are observed).[48] To ensure the reliability and reproducibility of ICD analysis, it is necessary to confirm that the unfolding equilibrium is reached. In our ICD experiments, the fluorescence spectra were measured over time after the samples were freshly prepared. We noticed that, while unfolding of lysozyme and BSA reached an equilibrium within 1 h, the spectra of mAbX apparently stopped changing only after 16 hours (data not shown). To gain more insight of the chemical unfolding process of mAbX, we conducted DLS experiments to monitor evolution of protein size after addition of GuHCl. We chose two denaturant concentrations for the DLS experiments: the middle point of transition on the ICD curve in Figure 1, i.e., $C_{d1/2}$, and another point on the plateau of the ICD curve. These points represent the partially unfolded state, where half of the protein population is in the unfolded state, and the fully unfolded state, respectively.

The DLS results for mAbX are reported in Figures 2 (first 6 h) and S5 (additional measurements up to 48 h). Figures 2A and S5 show that the hydrodynamic radius, R_h, of the partially

DOI: 10.1021/acs.molpharmaceut.8b00690
Mol. Pharmaceutics 2018, 15, 4710−4721

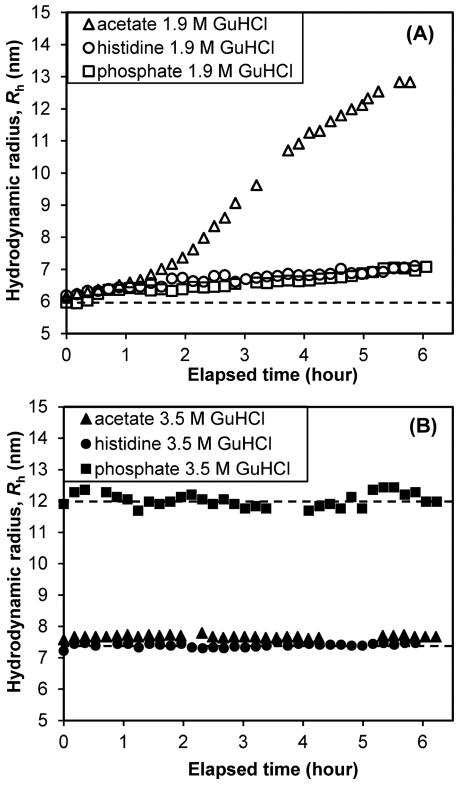

Figure 2. Evolution of hydrodynamic radius, R_h, of (A) the partially unfolded and (B) the fully unfolded mAbX during the first 6 h of unfolding after addition of GuHCl. The dashed lines are eye guides of the horizontal direction.

unfolded mAbX at $C_{d1/2}$ grows slowly over time. In contrast, the size of fully unfolded mAbX at high denaturant concentration becomes significantly larger than that of native protein upon addition of GuHCl and remains constant throughout the DLS experiments (Figure 2B). Even though the steady-state ICD curves of mAbX in all three buffers essentially overlap (Figure S2), the R_h of partially unfolded mAbX in acetate buffer has a kinetic profile very different from that in histidine and phosphate buffers, as shown in Figures 2A and S5. In these figures, we can see that growth of mAbX consists of two apparent stages. Within the first hour upon addition of GuHCl, the R_h of the antibody modestly increases from ~5.8 to ~6.4 nm at similar rates in different buffers. In the second stage, the size of protein in the acetate buffer starts to grow much earlier than when it would in the other two buffers. After ~20 h, the R_h of mAbX in acetate buffer reached a stable value at ~15.6 nm without further significant increase. At this point, we assumed that the partially unfolded mAbX in acetate buffer reached a steady state. In histidine and phosphate buffers, mAbX reached the steady state in ~30 h (Figure S5). The steady-state values of R_h of the native, partially, and fully unfolded proteins in the three buffers are summarized in Table 2.

One postulated mechanism of the observed two-stage growth kinetics is that the antibody started to partially unfold upon addition of GuHCl, resulting in the initial small increase of R_h, and then, during the second stage, the unfolded proteins formed submicron aggregates that have significantly larger size. This mechanism is supported by the scattering intensity profile (static light scattering) of the same course (Figure 3). The

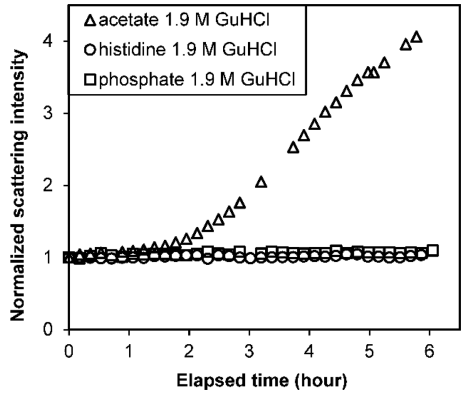

Figure 3. Normalized light scattering intensity profile for the DLS experiments in Figure 2A.

overall scattering intensity profile in Figure 3 resembles the R_h profile in Figure 2A. However, the first stage of R_h growth did not result in an obvious increase of scattering intensity in Figure 3. Protein unfolding per se changes the molecular volume but only has minor effects on the molecular mass. Because the scattering intensity mainly depends on the mass of scattering particles, the flat initial stage in Figure 3 is consistent with the protein unfolding process. When aggregation occurred in the second stage, the increase of the apparent molecular mass of protein aggregates caused the increase of scattering intensity, as shown in Figure 3 for the protein in acetate buffer.

Table 2. Hydrodynamic Radii, R_h, of the Native and Chemically Unfolded Proteins[a]

		R_h (nm) of proteins in unfolding experiments		
proteins	GuHCl(M)	acetate	histidine	phosphate
mAbX	0	5.80 ± 0.02	5.85 ± 0.04	6.16 ± 0.05
	1.90	15.60 ± 0.06[b]	12.05 ± 0.04[b]	11.9 ± 0.1[b]
	3.50	7.7 ± 0.1	7.39 ± 0.08	12.0 ± 0.3
BSA	0	3.68 ± 0.03	3.64 ± 0.02	3.53 ± 0.03
	1.55	4.41 ± 0.06	4.16 ± 0.07	4.4 ± 0.2
	2.10	5.7 ± 0.3	5.9 ± 0.2	5.4 ± 0.1
lysozyme	0	1.9 ± 0.2	1.8 ± 0.2	2.0 ± 0.1
	4.18	2.8 ± 0.2	2.6 ± 0.2	2.5 ± 0.2
	5.10	3.7 ± 0.4	2.6 ± 0.1	2.7 ± 0.2

[a]The proteins are partially unfolded at the lower GuHCl concentration and fully unfolded at the higher GuHCl concentration. [b]The R_h values of partially unfolded mAbX were taken at a steady state after incubation.

DOI: 10.1021/acs.molpharmaceut.8b00690
Mol. Pharmaceutics 2018, 15, 4710−4721

On the contrary, such an increase of scattering intensity has not been observed for fully unfolding of antibody.

The unfolding-aggregation mechanism can also explain why the apparent growth of R_h was observed for the partially unfolded antibody (Figure 2A) but not for the fully unfolded protein (Figure 2B). At denaturant concentration corresponding to partial unfolding (1.9 M), mAbX slowly unfolded and formed submicron aggregates in all three buffers as shown in Figures 2A and S5. At high denaturant concentration, protein unfolding is expected to be fast. Initial increase in protein size was not observed in Figure 2B, because the protein unfolding process was completed during the time of DLS sample preparation (~1 min). The high denaturant concentration also contributes to solubilizing the denatured protein, thereby suppressing aggregation. Therefore, the R_h of fully unfolded mAbX in acetate and histidine buffers are substantially lower than those of the small aggregates of partially unfolded mAbX (Table 2). In phosphate buffer, the fully unfolded mAbX formed particles of ~12 nm, comparable to that of partially unfolded protein (Figure 2B). The aggregation of mAbX in the phosphate buffer at high denaturant concentration also completed rapidly and did not lead to further increase of R_h during DLS measurement in Figure 2B.

Our DLS experiments revealed submicron aggregation of the antibody in the presence of GuHCl. Such protein aggregation is seemingly counterintuitive. GuHCl is a strong chaotropic salt that weakens electrostatic interactions, hydrogen bonds, van der Waals forces, and hydrophobic interactions. Disruption of these interactions causes protein unfolding and also prevents aggregation.[49−52] The driving force of protein aggregation in the presence of GuHCl is not obvious. However, the observations in our experiments can shed some light on the underlying interprotein interactions. Because the R_h profile in Figure 2 varies with pH, the driving force of aggregation could be electrostatic interactions between charged groups or hydrogen bonds that remain partially effective at relatively low GuHCl concentrations. In addition, the aggregation of partially and fully unfolded mAbX exhibits very different pH-dependence. This inconsistency can be explained by aggregation resulting from the interactions between individually charged functional groups, rather than the overall net charge of the protein itself.

The results shown in Figures 2, 3, and S5 depict a complex pathway of chemical denaturation for large proteins like mAbs. According to our findings, caution needs to be used when evaluating conformational stability of mAbs by ICD analysis. First, the steady states of antibodies may take a long time to achieve, which could depend on both the protein and the formulation buffer conditions. To obtain reproducible ICD curves, the incubation time for reaching the steady state needs to be empirically determined for each protein formulation. The slow chemical unfolding and subsequent protein aggregation were only observed for mAbX and not for BSA and lysozyme (Figure S6, Table 2). Long ICD incubation time has also been reported for other mAbs in previous studies.[16] Another pitfall of ICD analysis for antibodies is the use of oversimplified models that assume an equilibrium is established between the native and the well-defined unfolded states. Our experiments indicate the existence of submicron protein aggregates instead of free unfolded mAb. To examine the effect of protein aggregation, ICD curves can be collected at different protein concentrations and analyzed using a model accounting for both unfolding and self-association equilibria.[53,54] However, the advanced model in the previous studies only took into account the effect of aggregation on unfolding equilibrium; meanwhile, our results suggest that the denaturant concentration also affects aggregation of unfolded proteins. In addition, protein aggregation could cause changes in the fluorescence spectra and thereby further complicate the ICD analysis. Moreover, because the mechanism of protein unfolding depends on the denaturant, the results of ICD experiments using different denaturants, e.g., urea and GuHCl, could be significantly different and therefore not comparable.[16,49,52] As a result of the experimental and theoretical complexity described above, one should be prudent to conduct rigorous thermodynamic ICD analysis for antibodies.

It is important to note that the aggregation of antibody in the presence of denaturant may not reflect the propensity of unfolded proteins to undergo aggregation without denaturant. In Figure 2, we observed a substantial impact of GuHCl concentration on the aggregation. As a result of the presence of GuHCl, the submicron aggregates do not further grow. The ICD samples in all three buffers are free of large aggregates over long incubation periods (Figures 4 and S7). Next, we will study the protein aggregation after removal of the chemical denaturant.

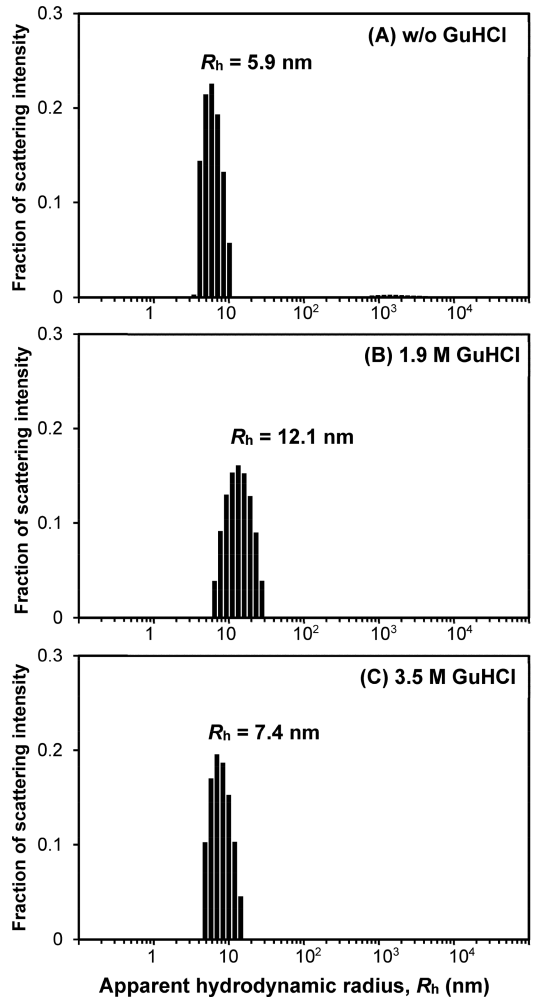

Figure 4. Distribution of hydrodynamic radii of (A) native mAbX, (B) aggregates of partially unfolded mAbX, and (C) fully unfolded mAbX in steady states in the pH 6.0 histidine buffer at 25 °C. The average R_h are labeled in the graphs.

DOI: 10.1021/acs.molpharmaceut.8b00690
Mol. Pharmaceutics 2018, 15, 4710−4721

3.3. Aggregation of mAbX after Removal of Chemical Denaturant. With the understanding of the chemical denaturation process for mAbX, we will now answer the following question: what happens to the partially and fully unfolded antibody in the absence of denaturant? This question is relevant to stability of real-life pharmaceutical formulations associated with partial unfolding. When the denaturant is removed, three scenarios may happen: the proteins refold back to the monomeric state, stay as metastable oligomers, or undergo further aggregation. We first employed a method based on dilution to rapidly reduce GuHCl concentration. The samples containing 40 mg/mL mAbX and 1.9 M ($C_{d1/2}$) or 3.5 M (fully unfolded) GuHCl were diluted 10 times with fresh buffer. After dilution, the GuHCl concentrations in the samples were reduced to 0.19 or 0.35 M, well below the level required for unfolding mAbX. For the fully unfolded mAbX samples, precipitation was observed in all three buffers upon dilution. By visual inspection, the amount of precipitates in phosphate buffer is greater than that in histidine buffer. Dilution with acetate buffer resulted in the least amount of precipitates. This trend is consistent with the distance of buffer pH from the pI of mAbX. On the contrary, the diluted samples of partially unfolded mAbX remained clear and were subjected to DLS measurements immediately after dilution (Figure 5). Figure 5A shows that the R_h of partially unfolded mAbX increased rapidly upon dilution. After ~2 h, the growth slowed but continued for at least 24 h (Figure S8A). The change of light scattering intensity in these experiments follows a similar kinetics profile (Figures 5B and S8B). The initial values of R_h in Figure 5A (>35 nm) are much larger than that of the metastable submicron aggregate before dilution (Table 2), likely because of the growth during sample preparation (~1 min). The diluted partially unfolded samples remained transparent for at least 2 weeks. Therefore, we conclude that partially unfolded mAbX undergo further submicron aggregation after removal of denaturant. Unlike the precipitation of fully unfolded mAbX, no obvious pH-dependence of aggregation has been observed for the partially unfolded protein.

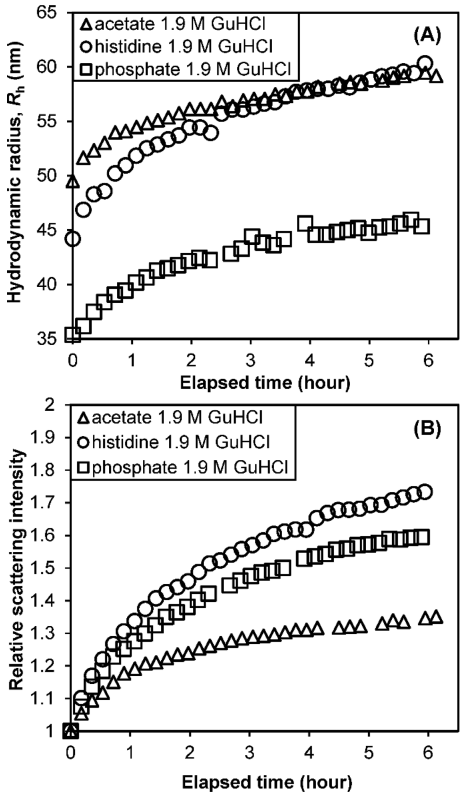

Figure 5. (A) Hydrodynamic radii of partially unfolded mAbX in three buffers as a function of time after GuHCl was diluted 10 times (0.19 M). (B) The relative scattering intensity as a function of time in the same experiments of (A).

We also conducted the dilution experiments for BSA and lysozyme (Figure S9). BSA formed submicron aggregates after dilution. However, these aggregates of BSA are much smaller than that of mAbX and do not grow over time (Figure S9A). The aggregates formed from fully unfolded BSA are systematically larger than those of partially unfolded BSA (Figure S9A). On the basis of the values of R_h, lysozyme always refolded into monomers with a slightly larger size than the native protein (Figure S9B). The R_h of mAbX, BSA, and lysozyme in the dilution experiments are summarized in Table 3. The comparison of these three proteins suggests that the propensity of denatured proteins to aggregate increases with protein size and degree of unfolding.

The dilution experiment provides a quick way to study the aggregation of chemically unfolded proteins. However, there are two potential limitations of this method. First, the residual GuHCl in the diluted sample could still affect subsequent aggregation. Second, the high initial protein concentration and fast reduction of GuHCl concentration could facilitate aggregation in a less reproducible manner. To eliminate these interferences, we removed the GuHCl from the protein samples by exhaustive dialysis against fresh buffer in a cold room at 4 °C. The buffer for dialysis was changed three times daily. Since dialysis is a gentle way to slowly remove GuHCl, the size of protein particles after dialysis should closely represent the equilibrium values. Photos of mAbX samples were taken after the 3 day dialysis (Figure 6). In Figure 6, the samples of partially unfolded mAbX in the three buffers were all transparent (Figure 6A,C,E). The fully unfolded mAbX in acetate buffer was also clear (Figure 6B). White precipitates were observed in the fully unfolded protein samples in histidine (Figure 6D) and phosphate (Figure 6F) buffers. Partially and fully unfolded BSA and lysozyme were also subjected to dialysis. All samples of BSA and lysozyme remained transparent after dialysis. All clear dialyzed samples were characterized by DLS. The R_h of the dialyzed proteins measured by DLS are summarized in Table 3. As shown in the table, the R_h of mAbX in the dialyzed samples are systematically smaller than those in the dilution experiments. This result is expected since the high initial protein concentration in dilution experiments and the quick reduction of GuHCl favor protein aggregation. For BSA and lysozyme, the R_h measured in the dialysis experiments are very similar to those in the dilution experiments, which may indicate absence of aggregation.

Overall, the DLS experiments of dialyzed samples agree with the experiments of diluted samples. The fate of unfolded proteins after removal of denaturant indeed depends on protein size and degree of unfolding. To summarize, the small protein lysozyme (14 313 Da) refolded into monomers. BSA (66 433 Da) formed small stable submicron aggregates. For large protein like mAbX (148 236 Da), the partially unfolded protein formed submicron aggregates even in the presence of denaturant, and these aggregates grew bigger but remained

DOI: 10.1021/acs.molpharmaceut.8b00690
Mol. Pharmaceutics 2018, 15, 4710−4721

Table 3. Hydrodynamic Radii of the Partially and Fully Refolded Proteins after Removal of Denaturant

		R_h (nm) 10× dilution			R_h (nm) dialysis		
proteins	original GuHCl (M)	acetate	histidine	phosphate	acetate	histidine	phosphate
mAbX	0	5.80 ± 0.02	5.85 ± 0.04	6.16 ± 0.05	----------	----------	----------
	1.90	66.1 ± 0.5[a]	69.9 ± 0.4[a]	52.8 ± 0.3[a]	23.8 ± 0.5	14.5 ± 0.2	21.1 ± 0.2
	3.50	precipitates	precipitates	precipitates	75.7 ± 0.5	precipitates	precipitates
BSA	0	3.68 ± 0.03	3.61 ± 0.09	3.53 ± 0.03	----------	----------	----------
	1.55	9.7 ± 0.1	10.9 ± 0.1	9.1 ± 0.1	9.9 ± 0.1	10.7 ± 0.1	9.78 ± 0.04
	2.10	12.8 ± 0.2	16.5 ± 0.2	13.6 ± 0.1	12.7 ± 0.1	16.7 ± 0.1	14.6 ± 0.2
lysozyme	0	1.9 ± 0.2	1.8 ± 0.2	1.9 ± 0.1	----------	----------	----------
	4.18	2.3 ± 0.1	2.4 ± 0.1	2.9 ± 0.2	2.0 ± 0.1	2.5 ± 0.2	2.0 ± 0.1
	5.10	2.9 ± 0.3	2.1 ± 0.1	2.3 ± 0.3	2.3 ± 0.2	2.1 ± 0.2	2.8 ± 0.2

[a]The R_h values of partially unfolded mAbX were taken at 24 h after dilution.

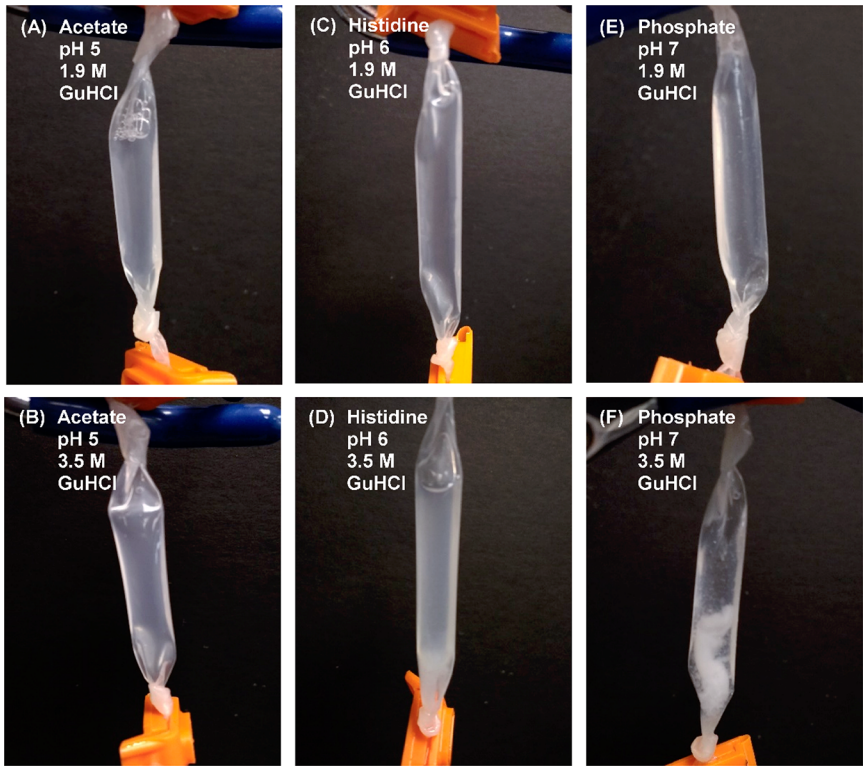

Figure 6. Dialysis bags containing 4 mg/mL chemically denatured mAbX samples in acetate, histidine, and phosphate buffers. The original protein samples before dialysis contained 1.9 and 3.5 M GuHCl. The photos were taken after the 3 day exhaustive dialysis. White aggregates were seen in (D) and (F).

soluble after removing the denaturant. The R_h distributions of these submicron aggregates are relatively narrow and free of large particles (Figures 7 and S10). When unfolding was extensive, the antibody precipitated out of solution upon removing denaturant. Aggregation of the fully unfolded mAbX exhibited strong pH-dependence, indicating a dominant effect of electrostatic interactions between charged groups of the protein. In contrast, the submicron aggregation observed for the partially unfolded mAbX did not show a consistent trend of pH-dependence. This difference suggests that formation of submicron aggregates is dictated by localized interactions and cannot be accounted for by the overall interactions between net charges. Furthermore, the submicron aggregation of mAbX in the presence of GuHCl was preceded by a lag time. Such delayed growth kinetics is often seen in nucleation-controlled protein aggregation. These nucleation phenomena are associated with collective interactions of proteins, e.g., aggregation of globular proteins without conformational changes[55,56] and amyloidogenesis of Aβ and prion proteins accompanied by formation of intermolecular β-strands.[25,27]

To learn more about the structural changes due to chemical denaturation and aggregation, we have compared the far-UV CD spectra of the native mAbX and the dialyzed partially unfolded protein (Figure 8). The CD spectra of native proteins show a negative band at around 217 nm, corresponding to the β-strands in the antibody. The denatured protein in the submicron aggregate also has a β-strand dominated secondary structure like that of the native protein (Figure 8, Table S1).[57] Despite the overall similarity of the CD spectra, the denatured mAbX appears to have a stronger band at 217 nm as compared to the native protein (Figure 8). This change may indicate the formation of additional β-strands during submicron aggregation, which is reminiscent of that found in the amyloid of Aβ and prion proteins.[58,59]

DOI: 10.1021/acs.molpharmaceut.8b00690
Mol. Pharmaceutics 2018, 15, 4710−4721

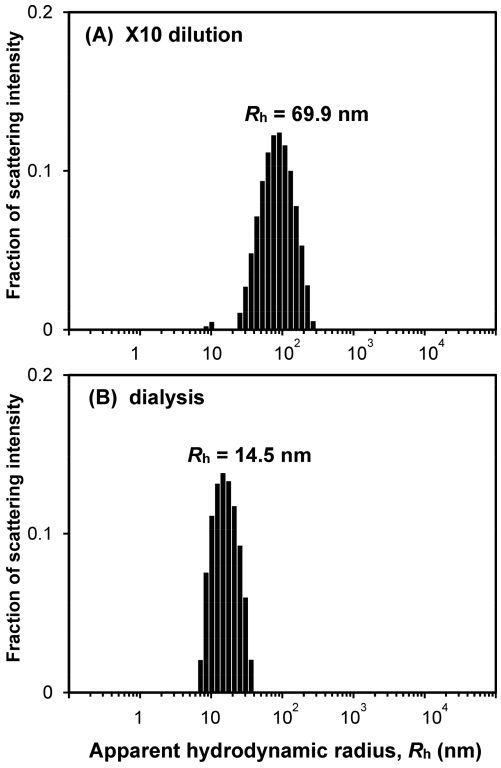

Figure 7. Distribution of hydrodynamic radii of partially unfolded mAbX in the pH 6.0 histidine buffer after removing GuHCl (A) by 10× dilution or (B) by dialysis. The average R_h are labeled in the graphs.

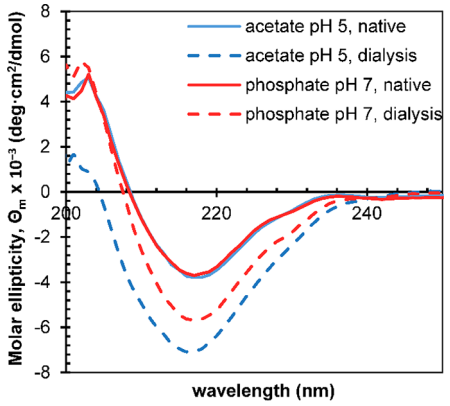

Figure 8. Far-UV CD spectra of the native mAbX and the dialyzed partially unfolded mAbX in acetate and phosphate buffers.

3.4. Comparison of Submicron Aggregation of Thermally and Chemically Denatured mAbX. Besides ICD, another method commonly used to evaluate conformational stability of proteins is thermal denaturation. Despite the different mechanisms of chemical and thermal denaturation, the subsequent aggregation of the unfolded proteins may share some similarity. In the last part of this study, we examined whether thermally denatured antibody also undergoes submicron aggregation. Heating protein solutions to high temperatures will lead to rapid protein precipitation. However, partial unfolding at moderately elevated temperatures may produce invisible aggregates. In addition, recent studies have raised questions on the relevance of the melting temperature (T_m) or onset temperature (T_{on}) obtained in DSC experiments to the actual long-term stability of biologics formulations.[8] Therefore, we think it is necessary to directly measure aggregation of partially unfolded antibodies for formulation development. To prepare the thermally denatured mAbX, we first conducted DSC experiments to determine the temperature needed for partial protein unfolding. The DSC heating curves of mAbX in Figure 9 have two peaks that are typical for

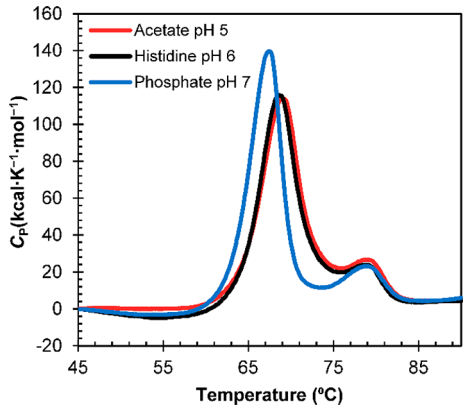

Figure 9. DSC heating curves of mAbX in acetate, histidine, and phosphate buffers.

full IgG antibodies.[60] The peak at ~79 °C corresponds to unfolding of the Fc domain. Figure 9 shows that the melting temperature of the Fc domain is not sensitive to the pH of buffer. The other peak in Figure 9 is located at ~67.5 °C in the pH 7 phosphate buffer and ~69 °C in the acetate and histidine buffers. This peak corresponds to unfolding of the Fab fragments. The two-step unfolding of mAb has not been observed in ICD curves (Figure 1). The apparent distinction between thermal and chemical unfolding is not surprising considering the different mechanisms of denaturation.

We then examined aggregation of thermally denatured mAbX by DLS experiments. The degree of thermal unfolding of the antibody was carefully controlled according to the results of DSC experiments. The antibody solutions were heated in a water bath from 40 °C at a rate of 0.2 °C per minute. The slow heating allows some equilibration time for unfolding. Protein precipitation started when the temperature was increased to above ~69 °C. Therefore, we quenched the samples with cold tap water as soon as the temperature reached 65 °C. The samples were immediately measured by DLS after quenching. On the basis of the hydrodynamic radii in Table 4, partial thermal denaturation of mAbX indeed produced submicron aggregates with sizes comparable to those from partial chemical denaturation. These aggregates formed during slow heating and did not further grow in the DLS experiments. Our study has confirmed that the thermally denatured antibody undergoes submicron aggregation when the antibody is partially unfolded.

4. CONCLUSIONS

In this work, we investigated the aggregation of a monoclonal antibody resulting from chemical denaturation. We found that the aggregation behavior of the denatured antibody mainly depended on the degree of denaturation. The partially unfolded antibody formed stable submicron aggregates even in the presence of denaturant. This submicron aggregation showed nucleation-controlled kinetics. After removing the

DOI: 10.1021/acs.molpharmaceut.8b00690
Mol. Pharmaceutics 2018, 15, 4710−4721

Table 4. Hydrodynamic Radii of the Partially Unfolded mAbX from Thermal and Chemical Denaturation[a]

	R_h (nm) of mAbX after partial denaturation		
	acetate	histidine	phosphate
thermal denaturation	10.6 ± 0.1	11.5 ± 0.2	21.2 ± 0.1 (13.5 ± 0.1)[b]
chemical denaturation (dialyzed)	23.8 ± 0.5	14.5 ± 0.2	21.1 ± 0.2

[a]The thermal denatured proteins were obtained by slowly increasing the solution temperature from 40 to 65 °C at the heating rate of 0.2 °C/min. [b]The number in the parentheses is from heating to 63 °C to account for the lower melting temperature in the phosphate buffer. The chemical denaturation data taken from Table 3 are from the unfolding with 1.9 M GuHCl followed by exhaustive dialysis.

denaturant, the aggregates grew but remained soluble. The submicron aggregation exhibited an irregular pH-dependence, indicating the importance of local electrostatic interactions on the aggregation of the partially denatured protein. In contrast, aggregation of fully denatured antibody was affected by pH in a manner consistent with the net charges of the protein. Far-UV CD experiments revealed that the aggregates of partially unfolded antibody retained the β-strand secondary structures. Finally, we found that the aggregation of the chemically and thermally unfolded antibody exhibit similar behavior, i.e., the propensities to aggregate increases with the degree of unfolding, and the partially unfolded proteins produce submicron aggregates.

Isothermal chemical denaturation has been widely used to evaluate protein conformational stability. Our study reveals the limitation of ICD thermodynamic analysis for large biologics, like mAbs, because of the invalid assumption of reversible unfolding. On the other hand, the ICD experiments, combined with the refolding/aggregation study, provide a practical means to compare the aggregation propensity of various antibody formulations. The degree of chemical denaturation can be controlled according to the ICD curves. The light scattering detection on dilution-induced aggregation is fast and sensitive. Using this approach, the stable submicron aggregates of partially denatured mAbX have been detected in the present work. Formation of such aggregates may shorten the shelf life of mAb formulations and raise safety concerns like adverse immunogenicity. The submicron aggregates could be overlooked in the widely used particle analyses based on microscopy or light obscuration techniques and therefore require particular attention in formulation development. In future studies, we will apply the ICD-induced aggregation analysis for more mAb molecules and explore the usefulness of this method to predict the long-term stability of antibody formulations.

■ ASSOCIATED CONTENT

Supporting Information

The Supporting Information is available free of charge on the ACS Publications website at DOI: 10.1021/acs.molpharmaceut.8b00690.

Additional figures and tables as noted in the text (PDF)

■ AUTHOR INFORMATION

Corresponding Authors

*Mailing Address: Ying Wang, Department of Chemistry, University of North Carolina Wilmington, Dobo 122, 4978 Cahill Drive, Wilmington, NC 28403, United States; E-mail: wangyy@uncw.edu.

*E-mail: pechenovs@medImmune.com.

ORCID

Ying Wang: 0000-0001-6370-4134

Present Addresses

[§]Jacob B. Rowe, Department of Molecular and Cellular Pharmacology, University of Miami Miller School of Medicine, Miami, FL 33136, United States

[‖]Jifeng Zhang, Sanofi, 1 The Mountain Road, Framingham, MA 01701, United States

Author Contributions

The manuscript was written through contributions of all authors. All authors have given approval to the final version of the manuscript.

Notes

The authors declare no competing financial interest.

■ ACKNOWLEDGMENTS

We thank Dr. Antje Pokorny Almeida at UNCW for assistance on the CD experiments. We thank Dr. Paulo F. Almeida, Ms. Elyse Tankoano, and Ms. Lucinda Boyd for assistance on the DSC experiments. This work is supported by a UNCW-MedImmune Collaboration grant.

■ ABBREVIATIONS

ICD, isothermal chemical denaturation; DLS, dynamic light scattering; DSC, differential scanning calorimetry; CD, circular dichroism; mAb, monoclonal antibody; GuHCl, guanidinium hydrochloride

■ REFERENCES

(1) Ratanji, K. D.; Derrick, J. P.; Dearman, R. J.; Kimber, I. Immunogenicity of therapeutic proteins: influence of aggregation. *J. Immunotoxicol.* **2014**, *11*, 99−109.

(2) Maas, C.; Hermeling, S.; Bouma, B.; Jiskoot, W.; Gebbink, M. F. A role for protein misfolding in immunogenicity of biopharmaceuticals. *J. Biol. Chem.* **2007**, *282*, 2229−2236.

(3) Joubert, M. K.; Luo, Q.; Nashed-Samuel, Y.; Wypych, J.; Narhi, L. O. Classification and characterization of therapeutic antibody aggregates. *J. Biol. Chem.* **2011**, *286*, 25118−25133.

(4) Freire, E. Differential Scanning Calorimetry. In *Protein Stability and Folding: Theory and Practice*; Shirley, B. A., Ed.; Humana Press: Totowa, NJ, USA, 1995; pp 191−218.

(5) Privalov, P. L.; Khechinashvili, N. N. A thermodynamic approach to the problem of stabilization of globular protein structure: a calorimetric study. *J. Mol. Biol.* **1974**, *86*, 665−684.

(6) Barone, G.; Giancola, C.; Verdoliva, A. DSC studies on the denaturation and aggregation of serum albumins. *Thermochim. Acta* **1992**, *199*, 197−205.

(7) Azuaga, A. I.; Dobson, C. M.; Mateo, P. L.; Conejero-Lara, F. Unfolding and aggregation during the thermal denaturation of streptokinase. *Eur. J. Biochem.* **2002**, *269*, 4121−4133.

(8) Brader, M. L.; Estey, T.; Bai, S.; Alston, R. W.; Lucas, K. K.; Lantz, S.; Landsman, P.; Maloney, K. M. Examination of thermal unfolding and aggregation profiles of a series of developable therapeutic monoclonal antibodies. *Mol. Pharmaceutics* **2015**, *12*, 1005−1017.

(9) Freire, E.; Schön, A.; Hutchins, B. M.; Brown, R. K. Chemical denaturation as a tool in the formulation optimization of biologics. *Drug Discovery Today* **2013**, *18*, 1007.

(10) Canchi, D. R.; Paschek, D.; Garcia, A. E. Equilibrium study of protein denaturation by urea. *J. Am. Chem. Soc.* **2010**, *132*, 2338−2344.

DOI: 10.1021/acs.molpharmaceut.8b00690
Mol. Pharmaceutics 2018, 15, 4710−4721

(11) Almeida, P. *Proteins: concepts in biochemistry*, 1st ed.; CRC Press, 2016.
(12) Ahmad, F.; Bigelow, C. C. Estimation of the free energy of stabilization of ribonuclease A, lysozyme, alpha-lactalbumin, and myoglobin. *J. Biol. Chem.* **1982**, *257*, 12935−12938.
(13) Santoro, M. M.; Bolen, D. W. Unfolding free energy changes determined by the linear extrapolation method. 1. Unfolding of phenylmethanesulfonyl alpha-chymotrypsin using different denaturants. *Biochemistry* **1988**, *27*, 8063−8068.
(14) Bolen, D. W.; Santoro, M. M. Unfolding free energy changes determined by the linear extrapolation method. 2. Incorporation of delta G degrees N-U values in a thermodynamic cycle. *Biochemistry* **1988**, *27*, 8069−8074.
(15) Greene, R. F., Jr.; Pace, C. N. Urea and guanidine hydrochloride denaturation of ribonuclease, lysozyme, alpha-chymotrypsin, and beta-lactoglobulin. *J. Biol. Chem.* **1974**, *249*, 5388−5393.
(16) Wafer, L.; Kloczewiak, M.; Polleck, S. M.; Luo, Y. Isothermal chemical denaturation of large proteins: Path-dependence and irreversibility. *Anal. Biochem.* **2017**, *539*, 60−69.
(17) Lapidus, L. J. Protein unfolding mechanisms and their effects on folding experiments. *F1000Research* **2017**, *6*, 1723.
(18) Mallamace, F.; Corsaro, C.; Mallamace, D.; Vasi, S.; Vasi, C.; Baglioni, P.; Buldyrev, S. V.; Chen, S. H.; Stanley, H. E. Energy landscape in protein folding and unfolding. *Proc. Natl. Acad. Sci. U. S. A.* **2016**, *113*, 3159−3163.
(19) Philo, J. S.; Arakawa, T. Mechanisms of protein aggregation. *Curr. Pharm. Biotechnol.* **2009**, *10*, 348−351.
(20) Morris, A. M.; Watzky, M. A.; Finke, R. G. Protein aggregation kinetics, mechanism, and curve-fitting: a review of the literature. *Biochim. Biophys. Acta, Proteins Proteomics* **2009**, *1794*, 375−397.
(21) Panchal, J.; Kotarek, J.; Marszal, E.; Topp, E. M. Analyzing subvisible particles in protein drug products: a comparison of dynamic light scattering (DLS) and resonant mass measurement (RMM). *AAPS J.* **2014**, *16*, 440−451.
(22) Lindgren, M.; Sörgjerd, K.; Hammarström, P. Detection and Characterization of Aggregates, Prefibrillar Amyloidogenic Oligomers, and Protofibrils Using Fluorescence Spectroscopy. *Biophys. J.* **2005**, *88*, 4200−4212.
(23) Chi, E. Y.; Krishnan, S.; Randolph, T. W.; Carpenter, J. F. Physical stability of proteins in aqueous solution: mechanism and driving forces in nonnative protein aggregation. *Pharm. Res.* **2003**, *20*, 1325−1336.
(24) Roberts, C. J. Therapeutic protein aggregation: mechanisms, design, and control. *Trends Biotechnol.* **2014**, *32*, 372−380.
(25) Lomakin, A.; Chung, D. S.; Benedek, G. B.; Kirschner, D. A.; Teplow, D. B. On the nucleation and growth of amyloid beta-protein fibrils: detection of nuclei and quantitation of rate constants. *Proc. Natl. Acad. Sci. U. S. A.* **1996**, *93*, 1125−1129.
(26) Kelly, J. W. The alternative conformations of amyloidogenic proteins and their multi-step assembly pathways. *Curr. Opin. Struct. Biol.* **1998**, *8*, 101−106.
(27) Wood, S. J.; Wypych, J.; Steavenson, S.; Louis, J.-C.; Citron, M.; Biere, A. L. α-Synuclein Fibrillogenesis Is Nucleation-dependent: IMPLICATIONS FOR THE PATHOGENESIS OF PARKINSON'S DISEASE. *J. Biol. Chem.* **1999**, *274*, 19509−19512.
(28) Blancas-Mejia, L. M.; Ramirez-Alvarado, M. Mechanism of Light Chain Amyloid Fibril Formation: Seeding-Nucleation and Polymerization Amyloid Formation and the Cross-Seeding Phenomenon. *Biophys. J.* **2016**, *110*, 398a.
(29) Andersen, C. B.; Manno, M.; Rischel, C.; Thorolfsson, M.; Martorana, V. Aggregation of a multidomain protein: a coagulation mechanism governs aggregation of a model IgG1 antibody under weak thermal stress. *Protein Sci.* **2010**, *19*, 279−290.
(30) Filipe, V.; Kukrer, B.; Hawe, A.; Jiskoot, W. Transient molten globules and metastable aggregates induced by brief exposure of a monoclonal IgG to low pH. *J. Pharm. Sci.* **2012**, *101*, 2327−2339.
(31) Brummitt, R. K.; Nesta, D. P.; Chang, L.; Kroetsch, A. M.; Roberts, C. J. Nonnative aggregation of an IgG1 antibody in acidic conditions, part 2: nucleation and growth kinetics with competing growth mechanisms. *J. Pharm. Sci.* **2011**, *100*, 2104−2119.
(32) Wu, H.; Kroe-Barrett, R.; Singh, S.; Robinson, A. S.; Roberts, C. J. Competing aggregation pathways for monoclonal antibodies. *FEBS Lett.* **2014**, *588*, 936−941.
(33) Kim, N.; Remmele, R. L., Jr.; Liu, D.; Razinkov, V. I.; Fernandez, E. J.; Roberts, C. J. Aggregation of anti-streptavidin immunoglobulin gamma-1 involves Fab unfolding and competing growth pathways mediated by pH and salt concentration. *Biophys. Chem.* **2013**, *172*, 26−36.
(34) Li, Y.; Ogunnaike, B. A.; Roberts, C. J. Multi-variate approach to global protein aggregation behavior and kinetics: effects of pH, NaCl, and temperature for alpha-chymotrypsinogen A. *J. Pharm. Sci.* **2010**, *99*, 645−662.
(35) Neergaard, M. S.; Nielsen, A. D.; Parshad, H.; De Weert, M. V. Stability of Monoclonal Antibodies at High-Concentration: Head-to-Head Comparison of the IgG1 and IgG4 Subclass. *J. Pharm. Sci.* **2014**, *103*, 115−127.
(36) Vermeer, A. W.; Norde, W. The thermal stability of immunoglobulin: unfolding and aggregation of a multi-domain protein. *Biophys. J.* **2000**, *78*, 394−404.
(37) Latypov, R. F.; Hogan, S.; Lau, H.; Gadgil, H.; Liu, D. Elucidation of acid-induced unfolding and aggregation of human immunoglobulin IgG1 and IgG2 Fc. *J. Biol. Chem.* **2012**, *287*, 1381−1396.
(38) Khawli, L. A.; Goswami, S.; Hutchinson, R.; Kwong, Z. W.; Yang, J.; Wang, X.; Yao, Z.; Sreedhara, A.; Cano, T.; Tesar, D.; Nijem, I.; Allison, D. E.; Wong, P. Y.; Kao, Y. H.; Quan, C.; Joshi, A.; Harris, R. J.; Motchnik, P. Charge variants in IgG1: Isolation, characterization, in vitro binding properties and pharmacokinetics in rats. *MAbs* **2010**, *2*, 613−624.
(39) Waldrep, J. C.; Noe, R. L.; Stulting, R. D. Analysis of human corneal IgG by isoelectric focusing. *Invest Ophthalmol Vis Sci.* **1988**, *29*, 1538−1543.
(40) Prin, C.; Bene, M. C.; Gobert, B.; Montagne, P.; Faure, G. C. Isoelectric restriction of human immunoglobulin isotypes. *Biochim. Biophys. Acta* **1995**, *1243*, 287−289.
(41) Alderton, G.; Ward, W. H.; Fevold, H. L. ISOLATION OF LYSOZYME FROM EGG WHITE. *J. Biol. Chem.* **1945**, *157*, 43−58.
(42) Kaplan, L. J.; Foster, J. F. Isoelectric focusing behavior of bovine plasma albumin, mercaptalbumin, and beta-lactoglobulins A and B. *Biochemistry* **1971**, *10*, 630−636.
(43) Nozaki, Y. The preparation of guanidine hydrochloride. *Methods Enzymol.* **1972**, *26*, 43−50.
(44) Vivian, J. T.; Callis, P. R. Mechanisms of tryptophan fluorescence shifts in proteins. *Biophys. J.* **2001**, *80*, 2093−2109.
(45) Sun, C.; Yang, J.; Wu, X.; Huang, X.; Wang, F.; Liu, S. Unfolding and refolding of bovine serum albumin induced by cetylpyridinium bromide. *Biophys. J.* **2005**, *88*, 3518−3524.
(46) Myers, J. K.; Pace, C. N.; Scholtz, J. M. Denaturant m values and heat capacity changes: relation to changes in accessible surface areas of protein unfolding. *Protein Sci.* **1995**, *4*, 2138−2148.
(47) Schon, A.; Clarkson, B. R.; Jaime, M.; Freire, E. Temperature stability of proteins: Analysis of irreversible denaturation using isothermal calorimetry. *Proteins: Struct., Funct., Genet.* **2017**, *85*, 2009−2016.
(48) Temel, D. B.; Landsman, P.; Brader, M. L. Orthogonal Methods for Characterizing the Unfolding of Therapeutic Monoclonal Antibodies: Differential Scanning Calorimetry, Isothermal Chemical Denaturation, and Intrinsic Fluorescence with Concomitant Static Light Scattering. *Methods Enzymol.* **2016**, *567*, 359−389.
(49) Camilloni, C.; Guerini Rocco, A.; Eberini, I.; Gianazza, E.; Broglia, R. A.; Tiana, G. Urea and guanidinium chloride denature protein L in different ways in molecular dynamics simulations. *Biophys. J.* **2008**, *94*, 4654−4661.
(50) England, J. L.; Haran, G. Role of solvation effects in protein denaturation: from thermodynamics to single molecules and back. *Annu. Rev. Phys. Chem.* **2011**, *62*, 257−277.

DOI: 10.1021/acs.molpharmaceut.8b00690
Mol. Pharmaceutics 2018, 15, 4710−4721

(51) Collins, K. D. Charge density-dependent strength of hydration and biological structure. *Biophys. J.* **1997**, *72*, 65−76.
(52) Monera, O. D.; Kay, C. M.; Hodges, R. S. Protein denaturation with guanidine hydrochloride or urea provides a different estimate of stability depending on the contributions of electrostatic interactions. *Protein Sci.* **1994**, *3*, 1984−1991.
(53) Schon, A.; Clarkson, B. R.; Siles, R.; Ross, P.; Brown, R. K.; Freire, E. Denatured state aggregation parameters derived from concentration dependence of protein stability. *Anal. Biochem.* **2015**, *488*, 45−50.
(54) Clarkson, B. R.; Schon, A.; Freire, E. Conformational stability and self-association equilibrium in biologics. *Drug Discovery Today* **2016**, *21*, 342−347.
(55) Annunziata, O.; Pande, A.; Pande, J.; Ogun, O.; Lubsen, N. H.; Benedek, G. B. Oligomerization and phase transitions in aqueous solutions of native and truncated human beta B1-Crystallin. *Biochemistry* **2005**, *44*, 1316−1328.
(56) Galkin, O.; Vekilov, P. G. Mechanisms of homogeneous nucleation of polymers of sickle cell anemia hemoglobin in deoxy state. *J. Mol. Biol.* **2004**, *336*, 43−59.
(57) Greenfield, N. J. Using circular dichroism spectra to estimate protein secondary structure. *Nature protocols* **2007**, *1*, 2876−2890.
(58) Rambaran, R. N.; Serpell, L. C. Amyloid fibrils: abnormal protein assembly. *Prion* **2008**, *2*, 112−117.
(59) Serpell, L. C. Alzheimer's amyloid fibrils: structure and assembly. *Biochim. Biophys. Acta, Mol. Basis Dis.* **2000**, *1502*, 16−30.
(60) Ionescu, R. M.; Vlasak, J.; Price, C.; Kirchmeier, M. Contribution of variable domains to the stability of humanized IgG1 monoclonal antibodies. *J. Pharm. Sci.* **2008**, *97*, 1414−1426.

DOI: 10.1021/acs.molpharmaceut.8b00690
Mol. Pharmaceutics 2018, 15, 4710−4721

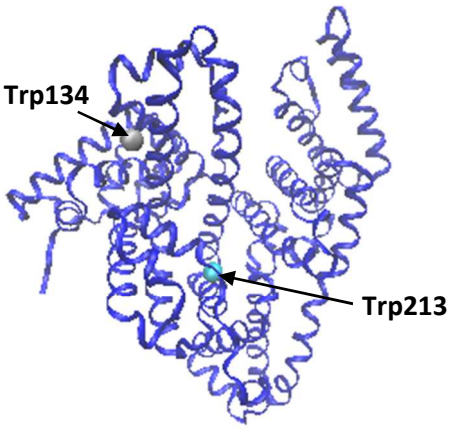

Figure S1. The X-ray structure of BSA (PDBe 4f5s) with two tryptophan residues represented by beads. The graphic was rendered using VMD software (University of Illinois at Urbana-Champaign).

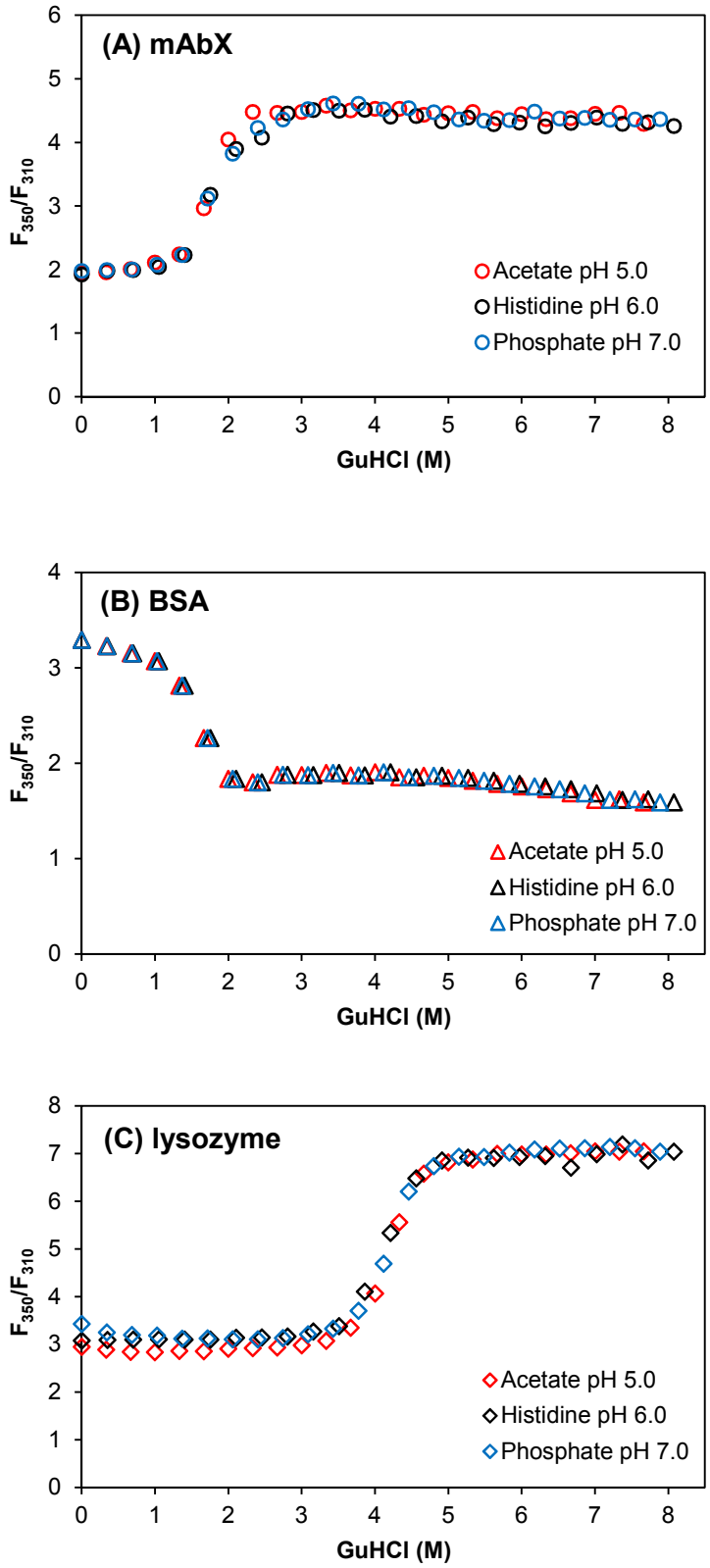

Figure S2. ICD curves of (A) mAbX, (B) BSA, and (C) lysozyme in three different buffers at 25 °C.

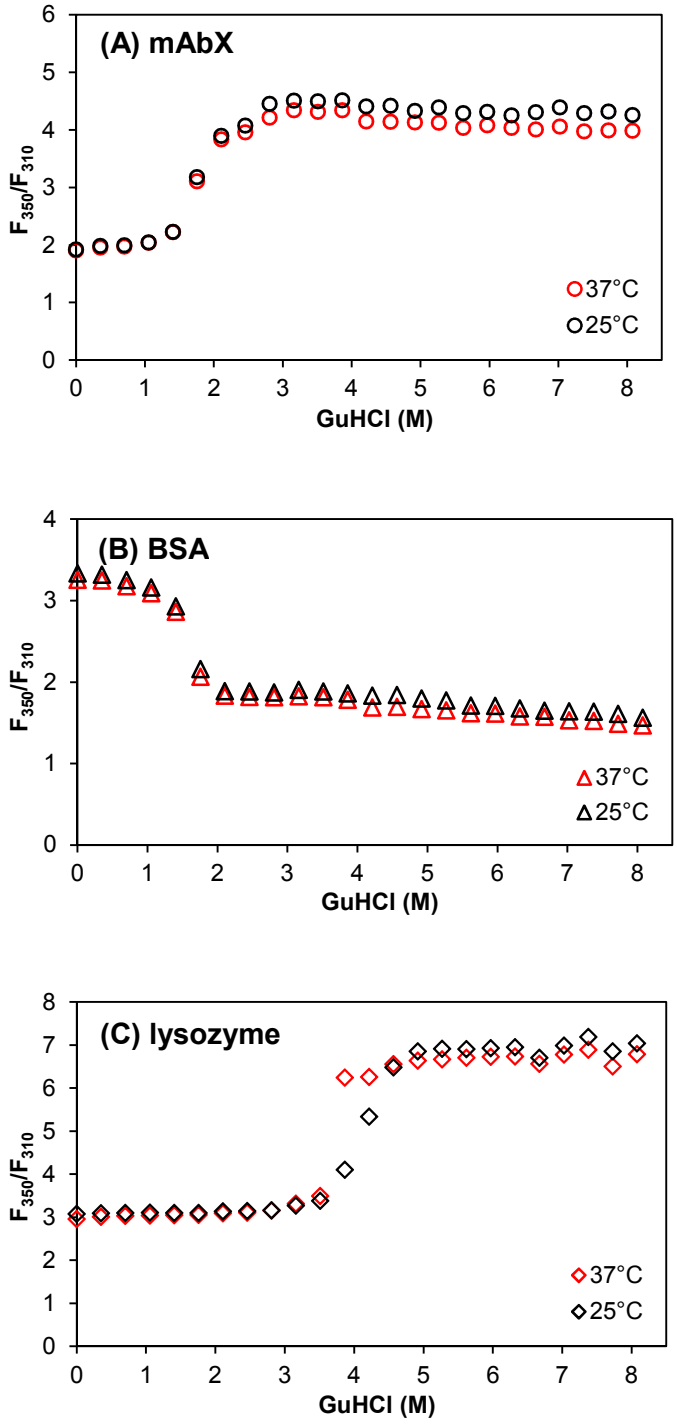

Figure S3. ICD curves of (A) mAbX, (B) BSA, and (C) lysozyme in histidine buffer at 25 °C and 37 °C.

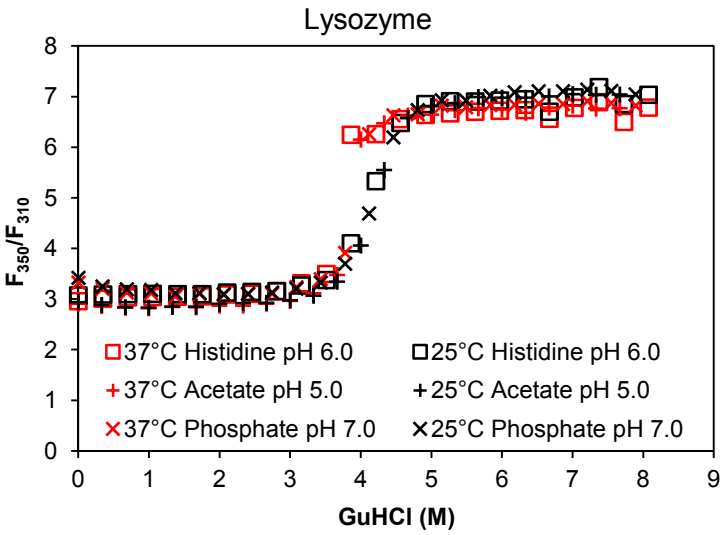

Figure S4. ICD curves of lysozyme in three different buffers at 25 °C and 37 °C.

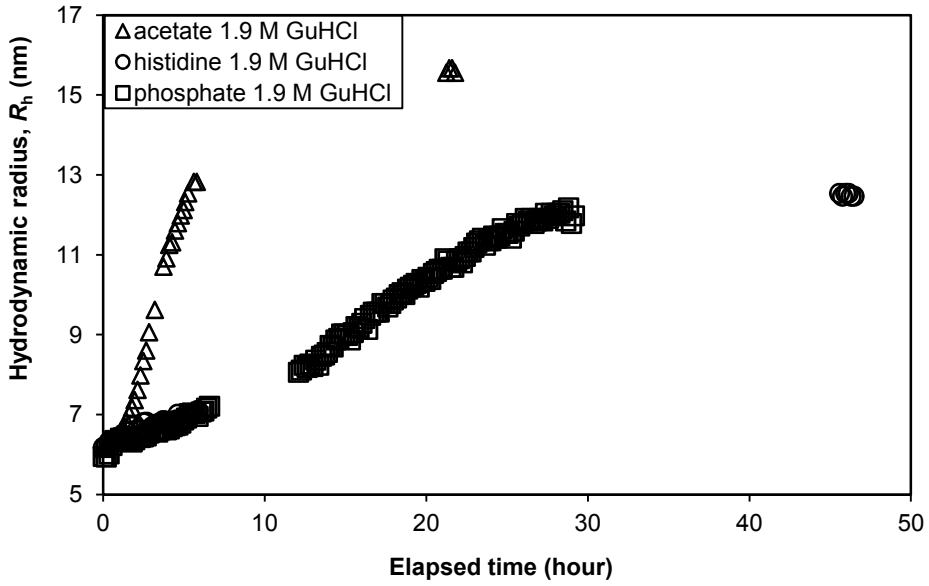

Figure S5. The hydrodynamic radii of partially unfolded mAbX slowly reach quasi-stable values after addition of GuHCl.

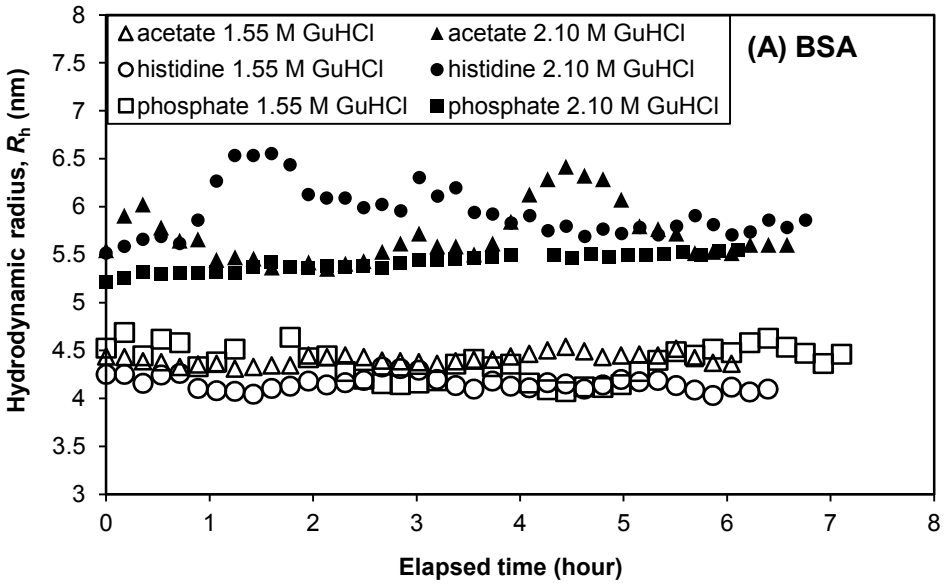

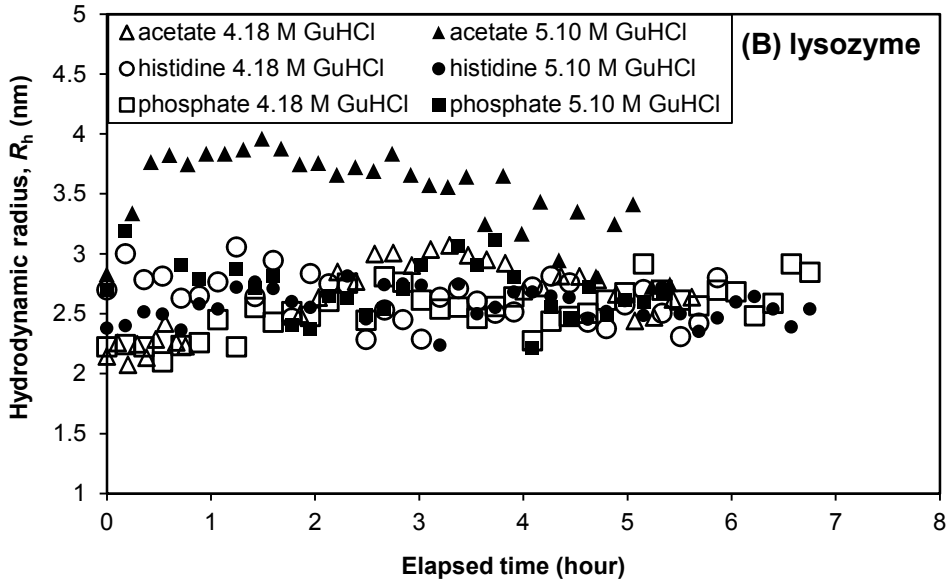

Figure S6. The hydrodynamic radii of partially and fully unfolded (A) BSA and (B) lysozyme monitored over time after addition of GuHCl.

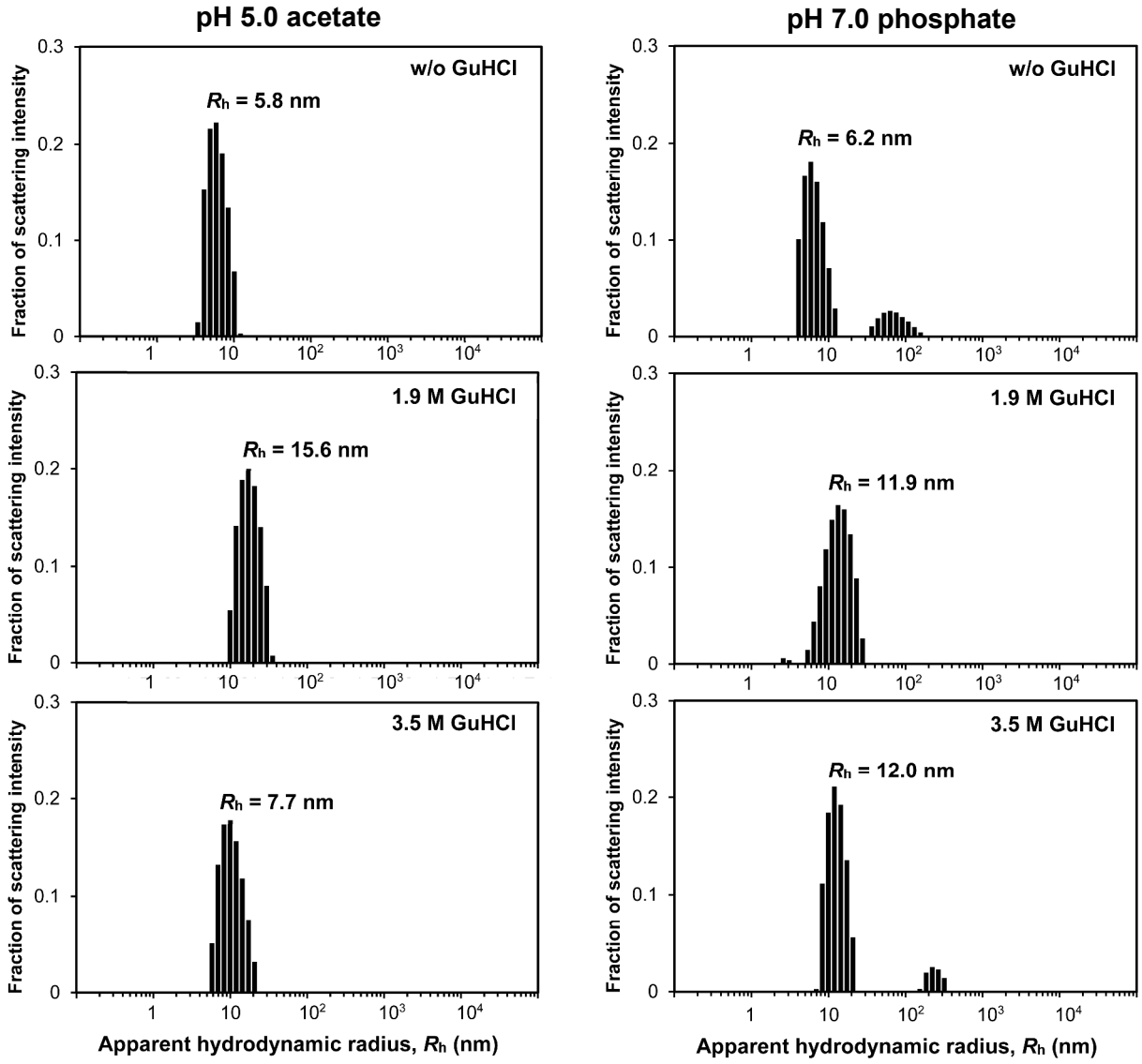

Figure S7. Distribution of hydrodynamic radii of native (top), partially unfolded (middle), and fully unfolded (bottom) mAbX in the pH 5.0 acetate buffer (left column) and the pH 7.0 phosphate buffer (right column) at 25 °C. The average R_h are labeled in the graphs.

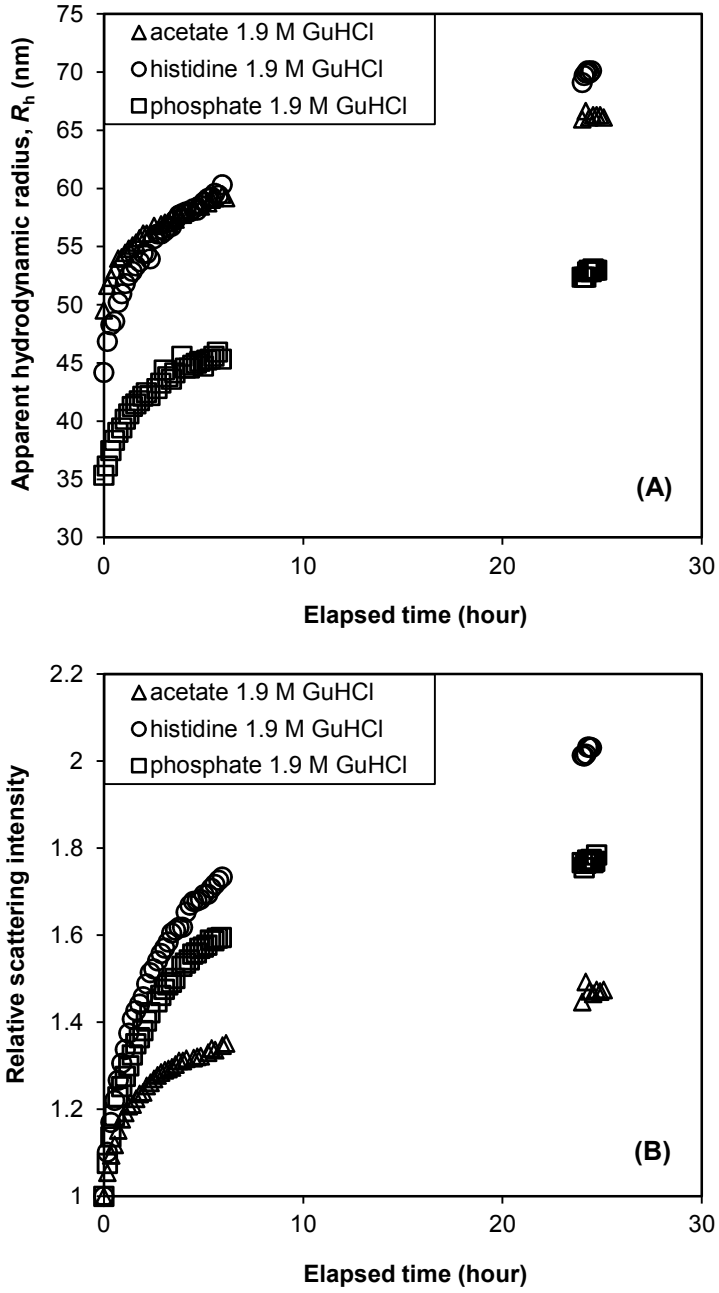

Figure S8. (A) Hydrodynamic radii of partially unfolded mAbX in three buffers as a function of time after GuHCl concentration was diluted 10 times (0.19 M). (B) The relative scattering intensity as a function of time in the same experiments of (A).

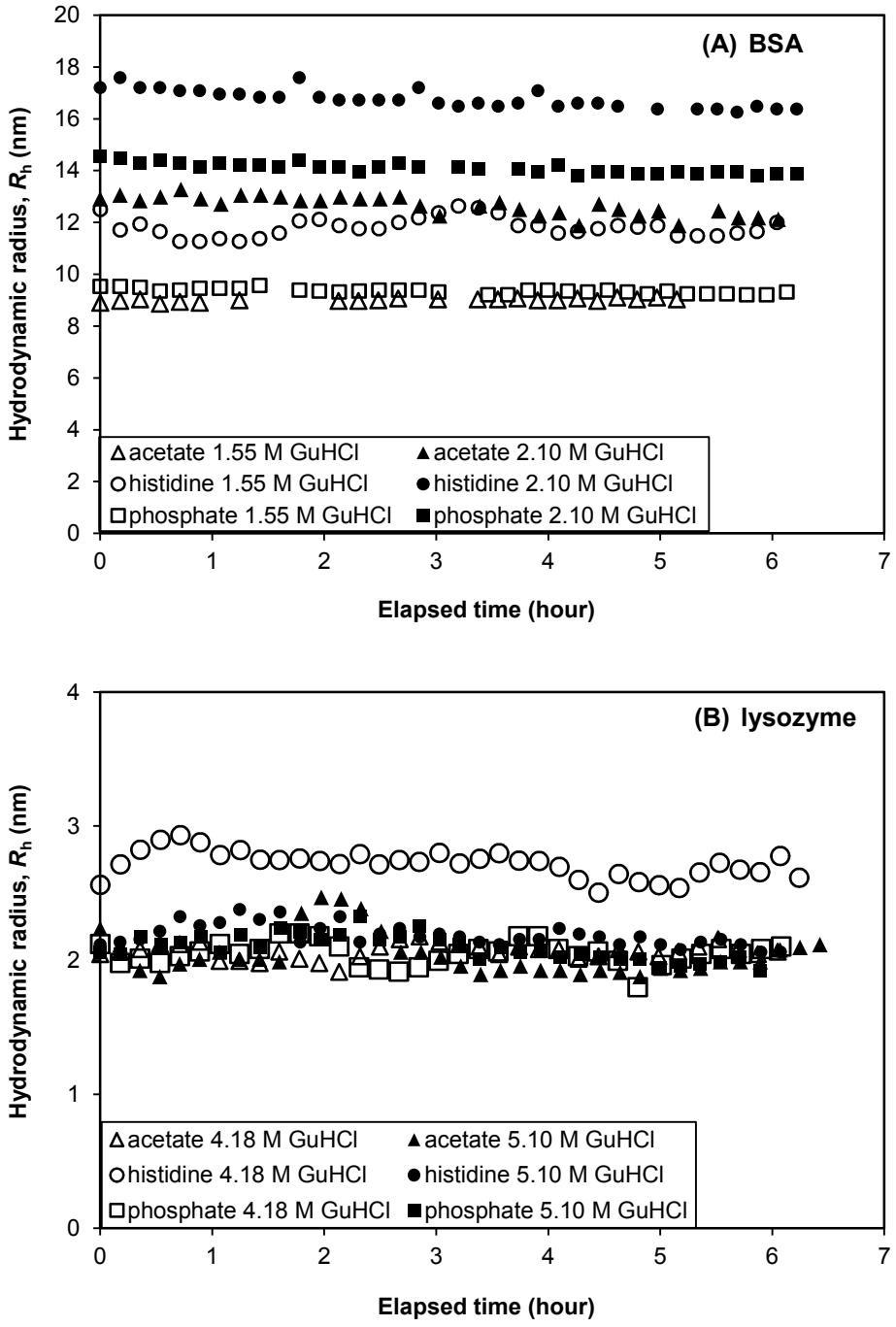

Figure S9. (A) Hydrodynamic radii of partially and fully unfolded BSA in three buffers as a function of time after GuHCl concentration was diluted 10 times (0.155 and 0.21 M). (B) Hydrodynamic radii of partially and fully unfolded lysozyme in three buffers as a function of time after GuHCl concentration was diluted 10 times (0.418 and 0.51 M).

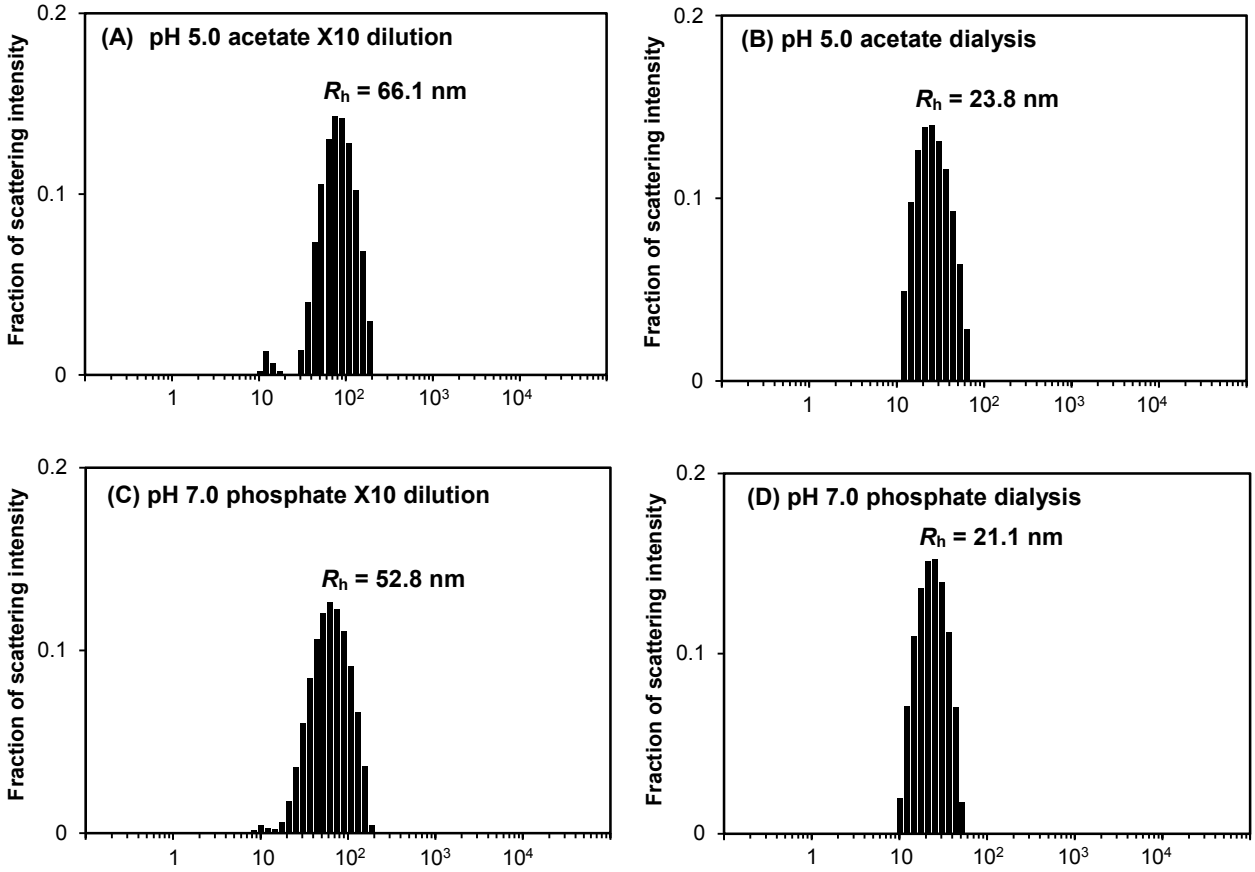

Figure S10. Distribution of hydrodynamic radii of partially unfolded mAbX in pH 5.0 acetate buffer and pH 7.0 phosphate buffer after removing GuHCl by x10 dilution or by dialysis. The average R_h are labeled in the graphs.

	Helix (regular)	Helix (distorted)	Strand (regular)	Strand (distorted)	Turn	Unorder	RMSD
Native acetate	0	0.03	0.27	0.14	0.21	0.35	0.03
Denatured acetate	0	0.03	0.24	0.14	0.23	0.36	0.03
Native phosphate	0	0.03	0.27	0.14	0.22	0.35	0.04
Denatured phosphate	0	0.03	0.26	0.14	0.22	0.35	0.05

Table S1. The secondary structures of native and dialyzed partially unfolded mAbX in acetate and phosphate buffers. The CD spectra were deconvoluted using the CDPro software package.[1] Three programs in this package, including CONTIN, CDSSTR and SELCON3, have produced similar results. The data obtained by CONTIN are presented in this table.

References:

1. Greenfield, N. J. (2006) Using circular dichroism spectra to estimate protein secondary structure, *Nature protocols 1*, 2876-2890.